JACS
JOURNAL OF THE AMERICAN CHEMICAL SOCIETY

ARTICLE

pubs.acs.org/JACS

Synthesis and Stabilization of Subnanometric Gold Oxide Nanoparticles on Multiwalled Carbon Nanotubes and Their Catalytic Activity

Leonor Alves,[†] Belén Ballesteros,[‡] Mercedes Boronat,[§] José Ramón Cabrero-Antonino,[§] Patricia Concepción,[§] Avelino Corma,*[,§] Miguel Angel Correa-Duarte,[∥] and Ernest Mendoza*[,†]

[†]Grup de Nanomaterials Aplicats, Centre de Recerca en Nanoenginyeria (CRNE), Universitat Politècnica de Catalunya, c/Pascual i Vila 17, 08028 Barcelona, Spain

[‡]Centre d'Investigació en Nanociència i Nanotecnologia (ICN-CSIC), Campus de la UAB, Edifici CM3, 08193 Bellaterra, Barcelona, Spain

[§]Instituto de Tecnología Química (UPV-CSIC), Universidad Politécnica de Valencia-Consejo Superior de Investigaciones Científicas, Av. de los Naranjos s/n, 46022 Valencia, Spain

[∥]Universidade de Vigo, Campus Universitario, 36310, Vigo, Spain

Supporting Information

ABSTRACT: Small gold nanoclusters in a very narrow size distribution (1.1 ± 0.5 nm) have been stabilized onto multiwalled carbon nanotubes (MWCNT). Theoretical studies supported by XPS and $^{16}O_2/^{18}O_2$ isotopic exchange experiments have shown that, on small gold nanoparticles (0.9−1.5 nm), dissociation of molecular O_2 and formation of a surface oxide-like layer is energetically favorable and occurs at room temperature, while O_2 recombination and desorption involves a larger activation barrier. CO titration experiments and theoretical studies demonstrate that the reactivity of the oxidized particles toward CO does not only depend on particle size but also on oxygen coverage. The oxidation−reduction process described is reversible, and the oxidized nanoparticles are active in the epoxidation of styrene with air.

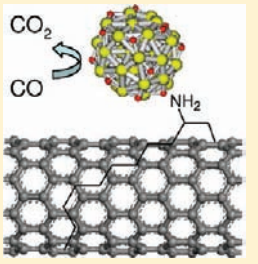

1. INTRODUCTION

There is much evidence in the literature showing that surface reactivity of nanoparticles dramatically changes when the size goes below a critical value.[1−7] This is the case for gold, which while inert as a metal can strongly interact with a variety of molecules when in the form of small nanoparticles,[8,9] becoming an active and selective catalyst for oxidations,[10−14] hydrogenations,[15−20] carbamoylation,[21] water gas shift,[22,23] hydrodechlorination, and carbon−carbon bond formation[24−27] reactions among others.

In the case of oxidation reactions, it is a matter of discussion as to how gold nanoparticles can activate oxygen. Some reports claim that bulk gold is not active to dissociate oxygen, though it can adsorb atomic oxygen delivered by molecular dissociation of NO_2 or O_2 on a hot filament or radicals provided by an oxygen plasma,[28−31] then being an effective catalyst.[32−34] Recent calculations based on density functional theory with unsupported Au nanoparticles indicate that there can be a critical size for gold nanoparticles to dissociate oxygen.[35−37] and that this is related not only to the larger amount of highly reactive low coordinated atoms in smaller particles, but also to differences in the metal electronic structure as particle size decreases.[38−40] Particle morphology also plays a role, as demonstrated by Herzing et al.,[41] who showed that small bilayer clusters of gold are active for CO oxidation, while monolayers of the same size are not. Experimental results from Goodman et al.[42] with a bilayer structure of gold that completely wets the $TiO_2(100)$ surface concluded that gold can be directly involved in the bonding and activation of O_2 without any influence of the support. In the case of Au_{55} clusters deposited on an inert support, Lambert et al.[43] concluded that small nanoparticles, and more specifically gold particles derived from 55 atoms, could dissociatively chemisorb O_2 to yield O adsorbed atoms. Very recently, Davis et al.[44] have demonstrated by means of $^{18}O_2$ and $H_2{}^{18}O$ labeling experiments that the oxygen atoms that are incorporated into the alcohol in the gold-catalyzed oxidation of ethanol and glycerol originate from hydroxide ions, and not from molecular oxygen.

EXAFS−XANES, as well as other evidence, indicates that partial oxidation of small gold nanoparticles (∼1.7 nm) can occur.[45−47] If this was the case, it appears to us that if one was able to synthesize very small gold nanoparticles (≤1 nm) within a very narrow crystallite size distribution, it should be possible not only to dissociate O_2 but to form a surface oxide-like layer that would be the interface where the catalytic oxidation process would occur. Furthermore, if this oxidized surface could undergo reversible oxidation−reduction cycles, one could assume an additional oxidation pathway on very small gold nanoparticles that could be assimilated to a Mars van Krevelen (MVK) mechanism,[48] where

Received: March 29, 2011
Published: June 02, 2011

Scheme 1. Schematic Representation of the Mars van Krevelen Mechanism

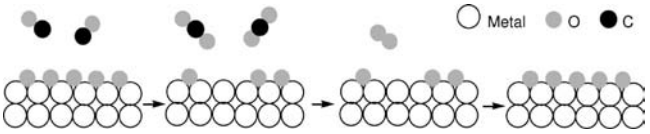

the oxygen from the oxide overlayer would be transferred to the reactant to be oxidized, while molecular oxygen would dissociate on the very small gold nanoparticles, regenerating the surface gold oxide-like layer (see Scheme 1).

Therefore, it can be of interest to prove the ability of gold to perform the dissociation of oxygen, the existence or not of a critical size for formation of a surface oxide layer, the occurrence of oxygen transfer from the surface oxide to the reactant, and the reversibility of the redox cycle. To help answer the above questions it would be required to prepare very small nanoparticles with a very narrow size distribution, on a support that avoids particle agglomeration during the catalytic process. This is a key issue since, up to now, gold nanocluster stabilization methods based on chemical routes[49,50] suffer from a partial poisoning of the catalytic active sites by the stabilization agent. Other attempts have relied on gold evaporation methods on substrates, but the scaling up of the process is difficult.[51]

In the present work we have developed small gold nanoclusters in a very narrow size distribution (1.1 ± 0.5 nm) onto multiwalled carbon nanotubes (MWCNT). We show that, in the presence of oxygen, oxidation of gold at the surface of the nanoparticles occurs at low temperature in a reversible way, and this could be used for performing catalytic oxidations. However, the above-mentioned phenomena were not observed on larger particles (4 nm). The combination of spectroscopic, kinetic, and theoretical studies has allowed us to investigate and explain the phenomena occurring at the surface of gold nanoparticles.

2. EXPERIMENTAL SECTION

2.1. Synthesis. The synthetic route to obtain stable CNT-supported gold nanoclusters starts by wrapping the CNTs with the polyelectrolyte polyallylamine hydrochloride (PAH). Multiwalled CNTs (Nanocyl NC3100) are dispersed in a 1 wt % aqueous solution of PAH (Sigma-Aldrich) at pH = 9 to a concentration of 1 mg/mL. A combination of rapid stirring and ultrasonication is used to ensure the presence of dispersed individual nanotubes. Excess PAH is removed by vacuum filtration and successive washing with ultrapure water. Then, the CNTs are resuspended in water at pH = 9. The reaction to synthesize the gold nanoclusters consists of adding to 50 mL of CNT−PAH solution the adequate amount of $HAuCl_4$ aqueous solution (Sigma-Aldrich) to yield the desired metallic gold content, i.e., from 0.3 to 15 wt %. Finally, sodium citrate (Sigma-Aldrich) is also used as stabilizer and soft reducing agent. The presence of citrate in the final catalyst is crucial for the stability of the gold nanoparticles in order to avoid their aggregation under catalytic reaction conditions. However the amount of citrate ions should be optimized, since an excess of citrate ions lowers the accessibility of the reactants to the catalytic active sites, while a defect favors aggregation of the nanoparticles. In this sense, a molar ratio of citrate/gold of 2000 has been proved to be optimum under our reaction conditions. Notice that the whole synthetic process takes place at room temperature.

2.2. Characterization. HRTEM images were acquired using a JEOL JEM-2011 microscope operated at 200 kV. The FTIR spectra were collected with a FTS-40A Bio-Rad spectrometer equipped with a DTGS detector (4 cm^{-1} resolution, 32 scans). A quartz cell connected to a vacuum system with gas dosing facility has been used. Blank run experiments without sample have been performed in the IR cell in order to reject the contribution of gaseous CO_2. The samples were activated in vacuum (10^{-3}mbar) at 120 °C prior to the IR experiment. X-ray photoelectron spectroscopy (XPS) measurements were performed on a SPECS spectrometer equipped with a Phoibos 150 MCD-9 analyzer using non-monochromatic Mg Kα (1253.6 eV) X-ray source working at 50 W. The XPS spectrometer was calibrated by using the BE of the $Ag_{3d5/2}$ line at 368.2 eV, the $Cu_{2p3/2}$ line at 932.6 eV, and the $Au_{4f7/2}$ line at 84.0 eV with respect to the Fermi level. As an internal reference for the peak positions in the XPS spectra, the C_{1s} peak has been set at 284.5 eV. The samples for IR and XPS analysis were prepared by dropping a Au−CNT−water suspension onto a germanium disk (for IR spectroscopy) and onto a molybdenum plate (for XPS analysis) followed by air drying. Oxygen isotopic-exchange experiments were conducted using a quartz microreactor coupled to a quadrupole mass spectrometer (Omnistar, QMG 220 M1). The experiments were performed on 60 mg of the sample using 22 mL/min of a $^{16}O_2$:$^{18}O_2$:Ar mixture (2:2:18). Prior to the experiment, the samples were activated in argon at 120 °C. The concentration profiles of the exit gas composition were obtained by acquiring the mass spectra signals relative to $^{16}O_2$ (m/e = 32), $^{16}O^{18}O$ (m/e = 34), and $^{18}O_2$ (m/e = 36). Blank run experiments were performed using an empty reactor in order to check contributions of the gas-phase reactions and stability of the mass spectrometer.

Styrene epoxidation was carried out in a reinforced glass batch reactor (2.5 mL, SUPELCO) closed with Teflon septum and equipped with a pressure gauge and a side arm with an on−off lock. A microsyringe can be allowed to inject and withdraw liquid or gas through the lock. A 2 mg portion of the catalyst was added to a mixture of 2 mmol of styrene and 10 mL of toluene and kept under vigorously stirring. The reactor was sealed and evacuated three times with O_2. The reaction was performed at 100 °C and 0.5 bar overpressure of O_2. Reaction products were analyzed by gas chromatography using a Carbowax 20 M column.

2.3. Computational Details. A Au_{38} cluster having a typical cuboctahedral shape and 1 nm diameter was used as a model for the gold nanoparticles. It was placed in a 20 × 20 × 20 Å cubic box, and the positions of all atoms were fully relaxed. Then, an increasing number of oxygen atoms were placed in different positions on the surface of the Au_{38} cluster, and in all cases, the positions of all gold and oxygen atoms were fully relaxed. Interaction energies were calculated by subtracting the energy of the relaxed Au_{38} cluster, $E(Au_{38})$, and of n O atoms, $E(O)$, from the total energy of the cluster with adsorbed oxygens, $E(Au_{38}O_n)$, according to

$$E_{int} = E(Au_{38}O_n) - E(Au_{38}) - nE(O)$$

All calculations are based on density functional theory (DFT) and were carried out using the Perdew−Wang (PW91)[52,53] exchange-correlation functional within the generalized gradient approximation (GGA) as implemented in the VASP code.[54,55] The Kohn−Sham orbitals used to obtain the electron density were expanded in a plane wave basis set with a kinetic energy cutoff of 500 eV, and the effect of the core electrons was taken into account by means of the projected augmented wave (PAW) method.[56] All calculations were carried out at the Γ k-point of the Brillouin zone. The atomic positions were optimized by means of a conjugate-gradient algorithm until atomic forces were smaller than 0.01 eV/Å. Transition states were located using the DIMER algorithm[57,58] and the stationary points were characterized by pertinent frequency analysis calculations. Vibrational frequencies were calculated by diagonalizing the block Hessian matrix corresponding to displacements of the O atoms and the Au atoms in direct contact

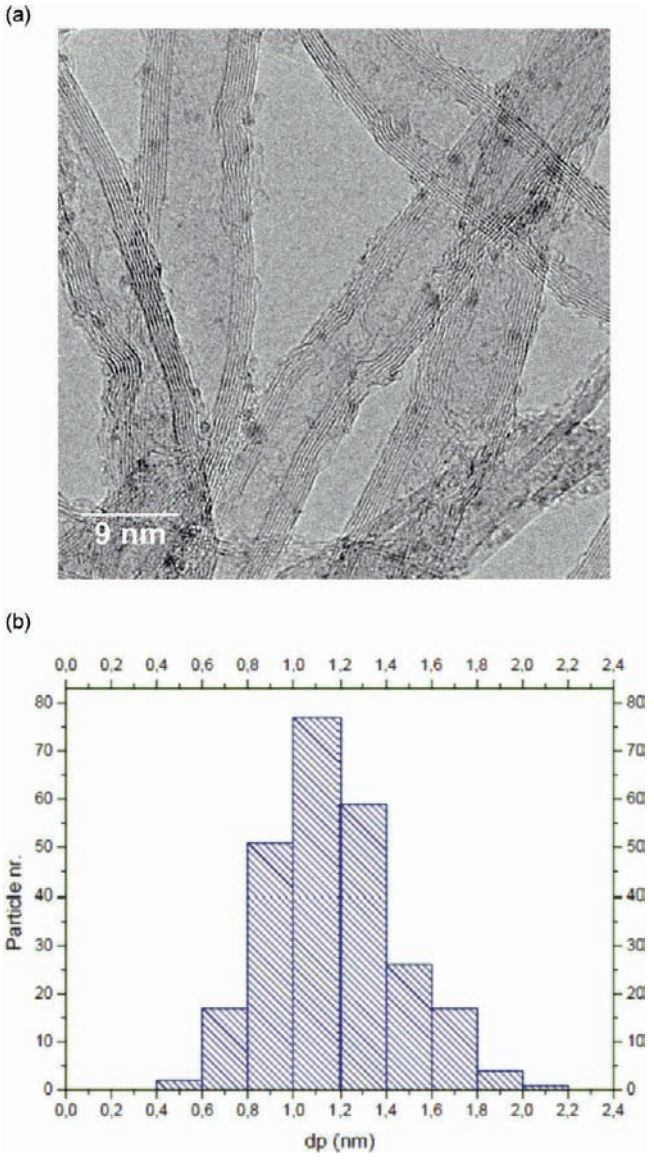

Figure 1. High-resolution TEM image of MWCNTs decorated with gold nanoclusters (a) and particle size distribution histogram for the 3Au−CNT sample containing 3% wt Au (b).

with O. Charge distributions were estimated using the theory of atoms in molecules (AIM) of Bader using the algorithm developed by Henkelman.[59,60]

3. RESULTS AND DISCUSSION

3.1. Synthesis and Characterization of Gold Nanoparticles. To clarify if gold oxide nanoparticles can be stabilized and if there is a critical nanoparticle size for formation of the oxide, it was necessary to first synthesize supported stable small nanoparticles within a very narrow size distribution. This was achieved by driving the gold nucleation and reduction on functionalized multiwalled carbon nanotubes (MWCNT), as described in the Experimental Section. In that way, small gold nanoclusters of 1.1 ± 0.5 nm were produced. Figure 1a shows a high-resolution transmission electron microscopy (HRTEM) image of the functionalized MWCNT with gold nanoclusters. The carbon atomic layers of the MWCNT and a large number of gold nanoclusters attached to their walls can be clearly identified. Notice the high density and homogeneous distribution of clusters onto the anisotropic carbon-based structures, which can be attributed to the heterogeneous nucleation caused by the presence of amino groups at the surface of the polyallylamine hydrochloride (PAH) coating the MWCNTs.[61] It is worth noting that the nanoclusters only form in the presence of sodium citrate, which is generally used as stabilizer and soft reducing agent. It should also be remarked that polymeric wrapping agents not containing amino groups, such as poly(4-sulfonate)styrene, hinder the formation of gold nanoclusters, even in the presence of sodium citrate, underlining the importance of the amino groups distribution on the surface of the supporting structure.

Table 1. Metal Loading (wt %), Mean Particle Diameter (nm), and XPS Data (eV) of Au−CNT Samples

sample	Au (wt %)[a]	D (nm)	BE Au $4f_{7/2}$ (eV)	α (eV)	Δε (eV)
0.3Au−CNT	0.3	0.9	86.3	n.d.[b]	
3Au−CNT	3	1.1	85.8	2096.3	0.45
6Au−CNT	6	1.5	85.6	2096.7	0.45
15Au−CNT	15	1.7	85.2	2096.4	−0.10
Au−CNT[c]	3	4	84.2	n.d.[d]	
Au foil		–	84.0	2099	

[a] Theoretical gold weight percent in the samples. [b] Because of the small signal for the Au $M_5N_{67}N_{67}$ Auger peak, reliable values cannot be obtained. [c] Prepared according to ref 62. [d] Noisy spectra.

The particle size distribution for a sample containing 3% wt gold is shown in Figure 1b. A narrow size distribution with very low dispersion, on the order of ±0.5 nm, is observed. Another interesting aspect of the preparation protocol is that the gold nanocluster size can be tailored from 0.9 to 1.7 nm by simply varying the amount of gold precursor between 0.3 and 15 wt % (see Table 1). For comparative purposes, AuNPs with a particle size of 4 nm have also been prepared. In this case, the nanoparticles were previously synthesized and then attached to the MWCNTs wrapped with PAH, as described in ref 62.

The electronic properties of the gold nanoparticles supported on MWCNT have been analyzed by XPS spectroscopy. The Au $4f_{7/2}$ binding energy (BE) of the Au−CNT samples with different gold contents, i.e., different particle size distributions, are given in Table 1. As observed, the BE increase by ∼2 eV relative to the bulk value of 84.0 eV when the gold particle size decreases to 0.9 nm. On the basis of the results with gold−organic compounds, a linear correlation between BE and oxidation state of Au could be established. Thus, BEs of 84.0, 84.6−85.1, and 85.9−86.3 eV have been assigned to Au^0, Au^+, and Au^{3+} species, respectively.[63] However, in the case of adsorbed metal particles on a metal oxide support, a shift to high binding energies at small cluster size has already been observed as a result of final state effects (reduced screening of the core hole, decreasing the kinetic energy of the ejected electrons).[64−66] Thus, in order to eliminate possible contributions due to final state effects, the Au auger parameter (α) has been calculated according to

$$\alpha = \mathrm{BE}(\mathrm{Au}\ 4f_{7/2}) + \mathrm{KE}(\mathrm{Au}\ M_5N_{67}N_{67}) \qquad (1)$$

where BE(Au $4f_{7/2}$) is the binding energy of the Au $4f_{7/2}$ electrons and KE(Au $M_5N_{67}N_{67}$) is the kinetic energy of the Au $M_5N_{67}N_{67}$ Auger electrons, and it has been included in Table 1. The value of α is independent of substrate charging and

it is a very sensitive probe of the physical and chemical environment of the analyzed atoms. Analyzing both the Au $4f_{7/2}$ BE shift (ΔBE) (relative to some reference state, typically the bulk metal) and the respective Au Auger parameter shift ($\Delta\alpha$), initial state contributions ($\Delta\varepsilon$) can be estimated with several approximations according to eq 2[62]

$$\Delta\varepsilon = \mathrm{BE} + (\Delta\alpha/2) \quad (2)$$

where the sign of $\Delta\varepsilon$ indicates whether the Au atom mean charge increases or decreases. From both the BE and the Au α parameters listed in Table 1, positively charged gold metal species can be inferred as having a particle size between 0.9 and 1.5 nm, while above 4 nm "bulklike" gold species are observed. The influence of the citrate ions, necessary to stabilize the gold nanoparticles, on the Au$4f_{7/2}$ binding energy and on the charge of the gold metal species has also been investigated (see the Supporting Information). This influence has been found to be very small. Therefore, the positively charged gold species observed at small particle size (0.9−1.5 nm) could be associated with gold bonded to oxygen species. If this is the case and the oxygen in the "gold oxide" can be transferred in an oxidation reaction and then regenerated by O_2 dissociation on the surface, it should be able to perform, for instance, a series of cycles following Scheme 2.

Scheme 2. Reversible Oxidation−Reduction of the Gold Nanoparticle Surface[a]

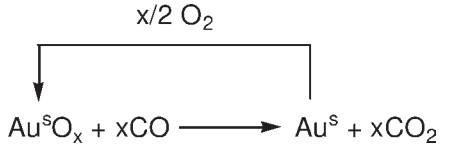

[a] Au^s denotes a surface Au atom.

3.2. IR and Isotopic $^{16}O_2-^{18}O_2$ Exchange Studies of the Reversible Redox Cycle. This cycle was followed by IR spectroscopy for the 3Au−CNT sample having 1.1 nm diameter (see Table 1). The CO_2 evolution due to CO titration at different temperatures is shown in Figure 2a−c. The CO_2 IR integration area decreases when increasing temperature, revealing a different reactivity of surface atomic oxygen species (Figure 2d). Since the oxygen coverage decreases with temperature, the different reactivity of the adsorbed oxygen species could be related to their different coverage. Thus, a lower reactivity is observed at lower oxygen coverage, as will be later explained by theoretical calculations. Titration experiments performed on Au particles above 4 nm do not show any CO_2 evolution (Figure 3), suggesting the absence of surface oxygen species, in agreement with the XPS data (Au BE and Au α similar to those observed on bulk Au). These results agree with the EXAFS−XANES data reported in the literature, showing that a partial oxidation of gold in air only occurs on small gold particles.[41−43]

At this point, several cycles of CO titration and sequential surface oxide regeneration in the presence of O_2 were performed and followed by IR spectroscopy. The CO_2 evolution during five consecutive days is shown in Table 2 for the 3Au−CNT sample with particle size of 1.1 nm. After exposing the sample to CO for a

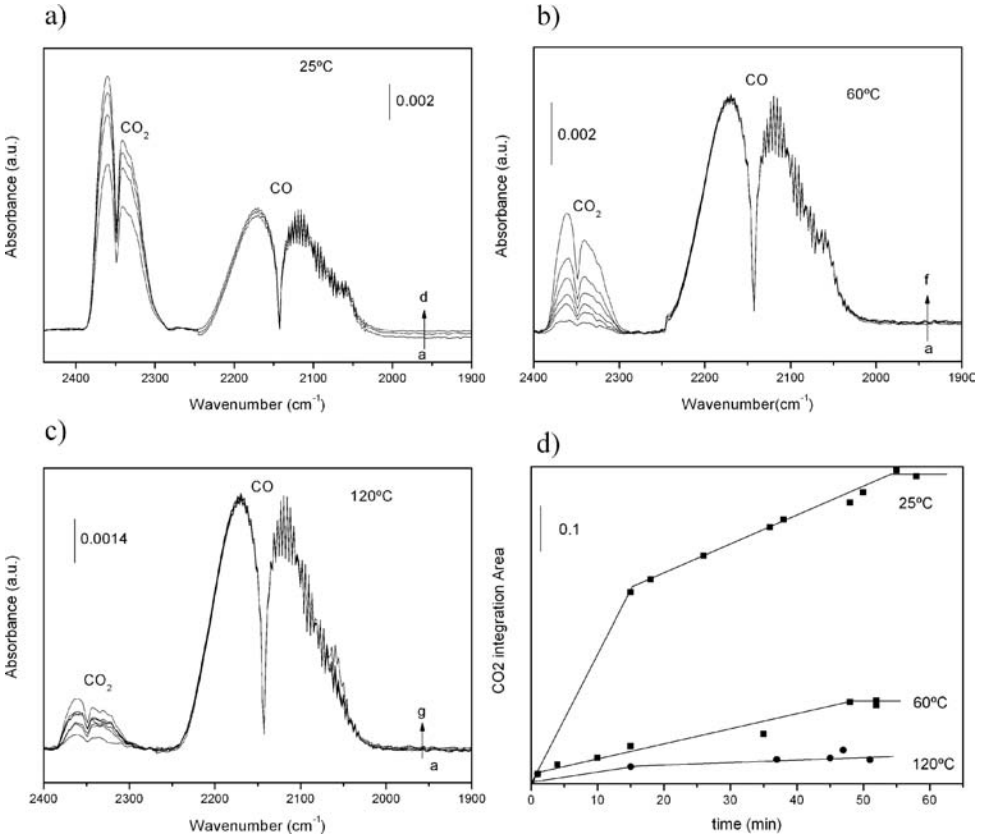

Figure 2. FTIR spectra of CO_2 evolution with time (0−60 min) after dosing 31 mbar of CO on the 3Au−CNT sample at reaction temperatures of (a) 25 °C, (b) 60 °C, and (c) 120 °C. (d) Time-resolved CO_2 formation at different reaction temperatures, determined by FTIR integration areas depicted in parts a−c.

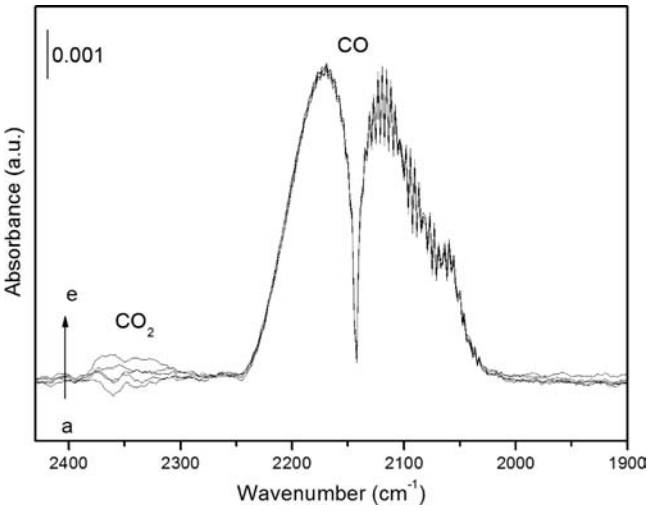

Figure 3. FTIR spectra of CO_2 evolution with time (0−74 min) after dosing 27.3 mbar of CO on the Au−CNT sample with 4 nm diameter at 25 °C.

Table 2. CO Titration of Surface "Au−Oxygen" Species on the 3Au−CNT Sample Followed by FTIR Spectroscopy

day	CO_2 area[a] (au)
1	0.31 ± 0.08
2	0.50 ± 0.09
3	0.32 ± 0.08
4	0.12 ± 0.06
5	0.44 ± 0.08

[a] CO_2 IR integration areas.

total of 6.5 h, practically all surface oxygen species had been titrated, and the CO_2 evolution in the last 30 min was very low. Overnight reoxidation of the sample with molecular oxygen at 25 °C restored practically its initial activity, as deduced from the CO_2 evolution on the following day shown in Table 2. Fluctuations in the amount of CO_2 produced are due to small changes in the average gold particle size (see Figure S4 of the Supporting Information). These results indicate that, if the gold particle size remains small (below 4 nm), these gold nanoparticles are able to dissociate molecular oxygen even at room temperature, this oxygen being involved in the catalytic cycle. It is important to note that in the case of Au nanoparticles larger than 4 nm, no surface oxygen species have been detected neither before nor after overnight reoxidation under an oxygen atmosphere.

Isotopic $^{16}O_2/^{18}O_2$ exchange experiments confirm the oxygen dissociation ability of gold nanoparticles, the extension of the isotopic exchange being particle-size dependent. In fact, Au nanoparticles of 1.1 nm (see Figure 4) showed oxygen dissociation (both $^{16}O_2$ and $^{18}O_2$) even at room temperature, while $^{16}O^{18}O$ release occurred at higher temperature (80 °C), probably due to a higher energetic barrier for desorption. On the other hand, Au NPs with particle size above 4 nm showed neither oxygen dissociation nor $^{16}O^{18}O$ release (see Figure 5).

In conclusion, from the above experimental results it can be inferred that Au NPs in the range of 0.9−1.7 nm are able to perform oxygen dissociation and to become oxidized. These oxygen species are highly reactive toward CO, and their reactivity

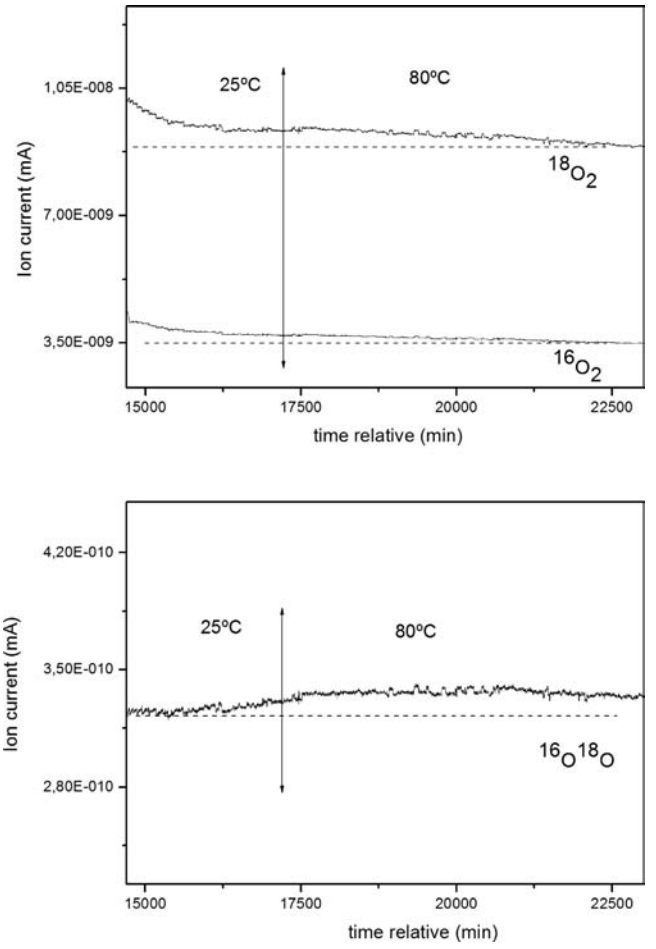

Figure 4. $^{16}O_2/^{18}O_2$ isotopic exchange at 25 and 80 °C on the 3Au−CNT sample with 1.1 nm diameter.

is coverage-dependent. Moreover, a cyclic oxidation−reduction process can be inferred, which is important from the point of view of their catalytic behavior in oxidation reactions. Once proven that (a) molecular O_2 dissociation occurs on small gold nanoparticles, (b) the particles are easily oxidized, (c) cyclic oxidation−reduction of the surface can easily occur, and (d) O_2 recombination and desorption is slower than O_2 dissociation, we have attempted to study the above-described process at the molecular level by means of theoretical calculations.

3.3. Theoretical Study. Previous theoretical studies have shown that small Au nanoparticles containing from 25 to 79 atoms and with particle diameter around 1 nm can dissociate molecular O_2 with low activation barriers.[35−37] However, these studies usually consider the dissociation of one isolated O_2 molecule into two separated O atoms and do not take into consideration the possibility of generating a surface oxide layer. We have now studied the adsorption of an increasing amount of O atoms on a Au_{38} nanoparticle having 1 nm diameter considering different distributions of O atoms for each coverage. The labeling of the positions considered and some of the structures obtained are depicted in Figure 6, other structures are depicted in Figures 7 and 8, and Table 3 summarizes the most relevant information relative to all systems investigated. The study of the $Au_{38}O$ model shows that atomic oxygen preferentially adsorbs on 3-fold hollow positions, with interaction energies (E_{int}) of

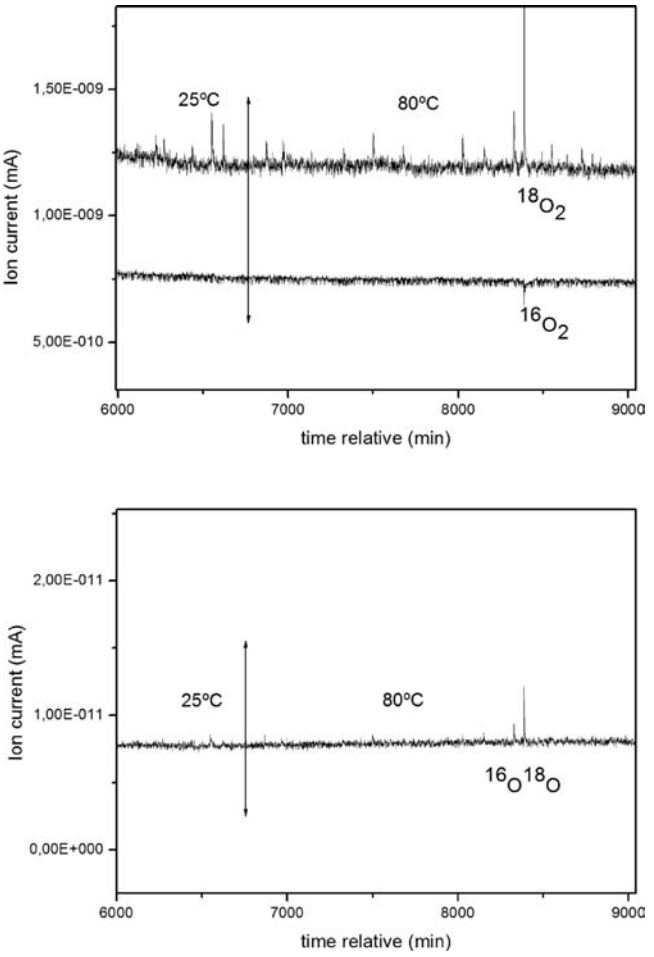

Figure 5. $^{16}O_2/^{18}O_2$ isotopic exchange at 25 and 80 °C on the Au−CNT sample with 4 nm diameter.

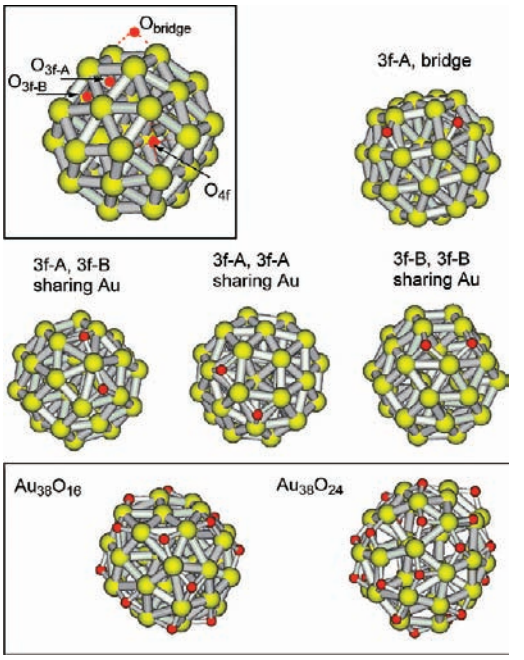

Figure 6. Different sites for atomic O adsorption on a Au_{38} nanoparticle.

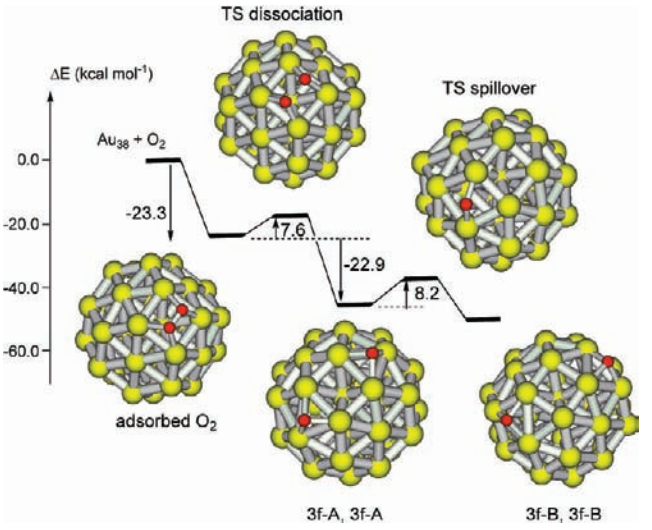

Figure 7. Calculated energy profile for O_2 dissociation and spillover of atomic O on a clean Au_{38} nanoparticle.

26−28 kcal/mol, but adsorption on bridge or 4-fold hollow positions is also energetically very favorable. In all cases, the oxygen atoms become negatively charged by ∼−0.8 e, and the Au atoms in contact with the oxygen become positively charged by ∼0.2 e. The interaction energies calculated for two oxygen atoms placed on separated 3-fold hollow positions (structures 3f-A,3f-A and 3f-B,3f-B in Figure 7) are 23−25 kcal/mol and slightly lower for the 3f-A,bridge structure depicted in Figure 6. Again, the oxygen atoms bear a negative charge of ∼−0.8 e, and the Au atoms in contact with the oxygens become positively charged by ∼0.2 e. When the two oxygen atoms in the $Au_{38}O_2$ model are directly bonded to the same gold atom, their negative charge is again −0.8 e, but the net positive charge on the shared Au atom increases to 0.4−0.6 e. Moreover, the structures with a linear O−Au−O geometry (3f-A,3f-B and 3f-A,3f-A in Figure 6), similar to that found for Au^I complexes, are the most stable, with calculated interaction energies close to 30 kcal/mol per O atom. When the number of adsorbed oxygen atoms increases to four in the $Au_{38}O_4$ model and they are placed close to each other [see structures 3x(3f-A), 4f and 2x(3f-A),2x(3f-B) in Figure 8], the interaction energy per O atom decreases to 15−16 kcal/mol, but the charge distribution is similar to that described for the $Au_{38}O_2$ systems. The same holds for the $Au_{38}O_{16}$ system depicted in Figure 6, in which all O atoms are forming the most stable O−Au−O linear structures. In fact, considering that 32 out of the 38 atoms of the gold cluster are on the surface, the $Au_{38}O_{16}$ model describes a nanoparticle covered by a monolayer of gold oxide. Adding more O atoms to the nanoparticle results in a decrease in the calculated E_{int} values and in the appearance of highly positive gold atoms that are directly bonded to three oxygen atoms. However, if one compares the calculated average charge on the gold atoms, $\langle q_{Au} \rangle$, it is possible to see a clear trend that holds for the whole series of models with increasing oxygen coverage. That is, each adsorbed oxygen creates a positive charge of 0.02 e on average on the gold atoms of the nanoparticle. This means that the gold nanoparticles of 0.9−1.7 nm, for which a mean positive charge has been experimentally obtained from BE and auger parameters, are covered by an oxide-like monolayer such as that simulated with the $Au_{38}O_{16}$ and $Au_{38}O_{24}$ models.

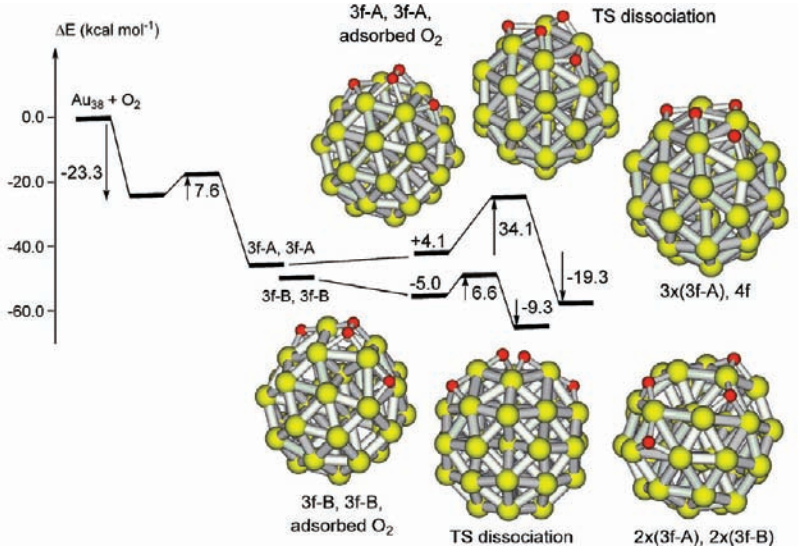

Figure 8. Calculated energy profiles for O_2 dissociation on a partially O-covered Au_{38} nanoparticle.

Table 3. Interaction Energies Per Adsorbed Oxygen Atom (E_{int}, kcal mol^{-1}), Average Net Atomic Charge on Each Oxygen Atom ($\langle q_O \rangle$), Average Net Atomic Charge on Each Au Atom of the Particle ($\langle q_{Au} \rangle$), and Largest Positive Charge on a Au Atom of the Particle ($q_{Au\,max}$, e) Calculated for Adsorption of One, Two, Four, 16, and 24 Oxygen Atoms at Different Sites on a Au_{38} Nanoparticle

system	site	E_{int} (kcal/mol)	$\langle q_O \rangle$	$\langle q_{Au} \rangle$	$q_{Au\,max}$
$Au_{38}O$	3f-A	−26.0	−0.817	0.021	0.226
	3f-B	−27.6	−0.826	0.022	0.232
	4f	−20.2	−0.785	0.021	0.196
	bridge	−22.9	−0.767	0.020	0.223
$Au_{38}O_2$	3f-A, 3f-A	−23.1	−0.830	0.044	0.247
	3f-A, bridge	−20.0	−0.795	0.042	0.249
	3f-A, 3f-B, sharing Au	−28.8	−0.836	0.044	0.469
	3f-A, 3f-A, sharing Au	−26.8	−0.841	0.044	0.560
	3f-B, 3f-B	−25.4	−0.809	0.043	0.220
	3f-B, 3f-B, sharing Au	−20.7	−0.797	0.042	0.417
$Au_{38}O_4$	3x(3f-A), 4f	−15.3	−0.781	0.084	0.674
	2x(3f-A), 2x(3f-B)	−16.2	−0.787	0.083	0.505
$Au_{38}O_{16}$		−15.0	−0.798	0.336	0.574
$Au_{38}O_{24}$		−8.7	−0.776	0.490	0.838

Figure 7 shows the energy profile corresponding to dissociation of one O_2 molecule on a clean Au_{38} nanoparticle following the reaction path involving the lowest activation barrier.[37] As previously described, molecular O_2 adsorbs with a bridge−bridge conformation on a (100) facet of the nanoparticle. This adsorption mode results in a large degree of the electron density transfer from gold to the π^* molecular orbitals of O_2, which weakens the O−O bond and facilitates its dissociation. The calculated activation energy is low, 7.6 kcal/mol, and the process is highly exothermic. The stability of citrate ions anchored on the gold nanoparticles and their influence on the adsorption and dissociation of molecular O_2 were theoretically investigated (see Figure S2 and Table S2 in the Supporting Information). It was found that the main effect of citrate ions is to block the gold active sites, but not to modify the nature of the gold−oxygen interaction. After dissociation of molecular O_2, the two oxygen atoms are placed in separated 3f-A hollow positions, but the activation energy necessary to spill over to a more stable 3f-B position is not too high, 8.2 kcal/mol, and therefore it can be assumed that oxygen atoms move easily on the particle surface. Moreover, according to the reaction path depicted in Figure 6, after dissociation of a first O_2 molecule, the active site consisting of four gold atoms arranged as in the (100) surface is not occupied by any

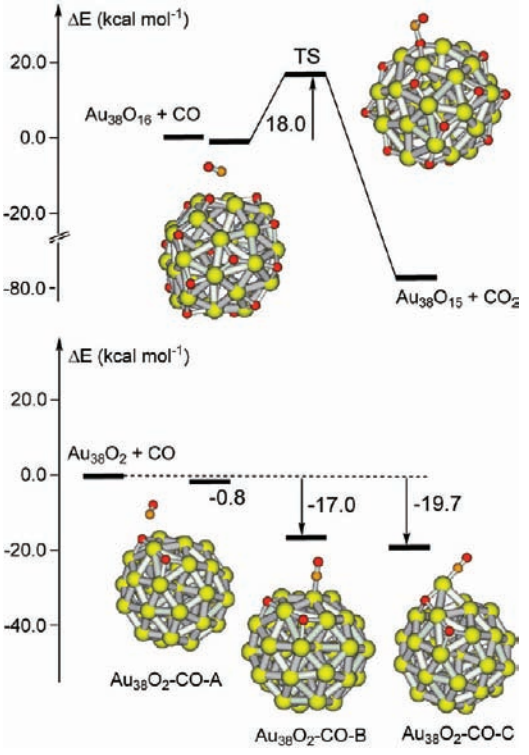

Figure 9. Calculated energy profiles for CO oxidation on a $Au_{38}O_{16}$ nanoparticle covered by an oxide layer (top) and on a partially O-covered $Au_{38}O_2$ nanoparticle (bottom).

Table 4. Epoxidation of Styrene on Au−MWCNT Samples

				% yield				
sample[a]	D (nm)	t (h)	conv (%)	benzald	epoxide	acetoph	benz acid	others
0.3Au−CNT	0.9	2	3.0	2.5	0	0	0	0.5
		4	11.7	8.2	0.6	0	0.4	2.5
		6	25.2	14.2	2.5	0.1	1.9	6.5
3Au−CNT	1.1	2	2.3	1.6	0	0	0	0.7
		4	9.0	5.7	0.8	0	0.3	2.2
		6	17.6	9.5	2.0	0.1	1.1	4.9
3Au−CNT[b]	1.1	2	1.2	0.9	0	0	0	0.3
		4	2.5	2.1	0	0	0	0.4
		6	11.1	7.3	0.8	0	0.4	2.6
15Au−CNT	1.7	2	1.3	1.1	0	0	0	0.2
		4	6.	4.3	0.3	0	0.1	1.3
		6	15.4	9.2	1.6	0.1	0.8	3.7
Au−CNT[c]	4	2	0	0	0	0	0	0
		4	0	0	0	0	0	0
		6	2.7	2.2	0	0	0	0.5
CNT	–	2	0	0	0	0	0	0
		4	0	0	0	0	0	0
		6	0	0	0	0	0	0

[a] Citrate/Au molar ratio 2000 in all samples except where noted. Reaction conditions: 6 mmol of styrene, 10 mL of toluene, 2 mg of Au−CNT sample, 1.5 bar of O_2, and 100 °C. [b] Citrate/Au molar ratio = 600. [c] Prepared according to ref 62.

oxygen atom but is free to dissociate a second O_2 molecule. As depicted in Figure 8, adsorption of a O_2 molecule on the 3f-A,3f-A structure is not energetically favorable and its dissociation involves a large activation barrier. However, O_2 adsorption on the 3f-B,3f-B structure is exothermic by 5.0 kcal/mol, and the activation energy necessary to dissociate it is only 6 kcal/mol. Thus, there is a pathway for O_2 dissociation on partially oxygen covered nanoparticles that involves a low activation barrier and again leaves the four Au atoms of the active site free for subsequent dissociations. Assuming a cuboctahedral shape for the gold nanoparticles of ~1 nm diameter and considering that there are six active sites on each nanoparticle and that each active site can dissociate at least two O_2 molecules with low activation barriers, it can be concluded that it is possible and easy to reach a coverage of one monolayer oxide ($Au_{38}O_{16}$) and even more ($Au_{38}O_{24}$). With respect to oxygen recombination, the energy profile depicted in Figure 6 indicates that recombination of two O atoms adsorbed on a clean gold nanoparticle is difficult and involves an activation barrier of more than 30 kcal/mol. However, the process is much easier on the oxide-covered particles, for which the activation energy necessary to form a O_2 molecule by combining two oxygen atoms is 15.9 kcal/mol. This activation barrier is larger than that calculated for O_2 dissociation, in agreement with the experimental $^{16}O_2/^{18}O_2$ isotopic exchange experiments showing that oxygen dissociation occurs at room temperature while $^{16}O^{18}O$ release is not observed at temperatures below 80 °C.

Furthermore, these oxidized particles can be easily reduced, as suggested by the CO titration experiments. The energy profile for CO reaction with an oxide-covered $Au_{38}O_{16}$ nanoparticle and with a $Au_{38}O_2$ model was calculated, and the results are depicted in Figure 9. CO interaction with the $Au_{38}O_{16}$ model is weak, −0.8 kcal/mol, and

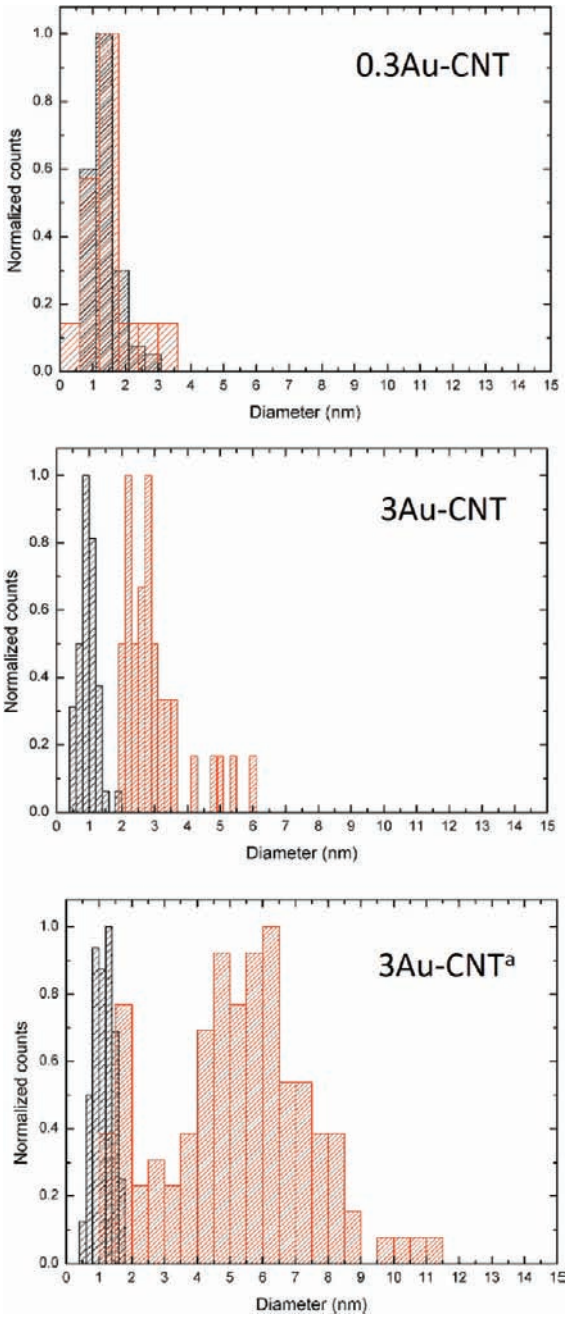

Figure 10. Particle size distributions determined from the TEM study of the 0.3Au−CNT (top), 3Au−CNT (center), and 3Au−CNT[a] (bottom) samples before (black) and after (red) catalytic test.

the molecule remains at 3.18 Å from the closest O atoms and at 3.78 Å from the closest Au atom, with the CO bond length being equivalent to that calculated for the isolated molecule. In the transition state one of the oxygen atoms of the oxide layer is being transferred to CO, with an optimized O−CO distance of 1.55 Å, while the CO bond slightly increases to 1.17 Å. The calculated activation barrier is 18.0 kcal/mol, and the resulting $Au_{38}O_{15} + CO_2$ system is 78.7 kcal/mol more stable than the initial reactants.

The situation is quite different on an almost clean gold nanoparticle. We considered the most stable 3f-A,3f-B structure to simulate a gold nanoparticle with only two oxygen atoms adsorbed on it and studied the adsorption of CO on different

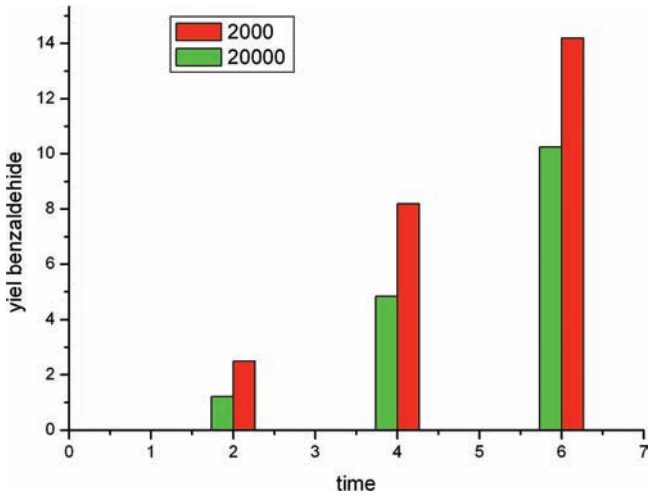

Figure 11. Yield to benzaldehyde at 2, 4, 6 h reaction time on 0.3Au−CNT sample at two different citrate/gold molar ratios (2000 and 20 000).

positions. The structures and interaction energies shown in Figure 9, bottom, indicate that CO does not interact with a Au atom directly bonded to two oxygens (structure $Au_{38}O_2$−CO−A) but remains above the particle at 3.07 Å from the positively charged Au atom. However, CO interacts strongly with either a neutral Au atom not in direct contact with an oxygen atom (structure $Au_{38}O_2$−CO-B), with a calculated interaction energy of −17.0 kcal/mol, or with a slightly positive Au atom that is directly bonded to only one O atom (structure $Au_{38}O_2$−CO−C). In this last case, a noticeable deformation of the particle occurs and the resulting structure is the most stable among all the considered systems. However, the high stability of these structures in which CO binds strongly to a gold atom ($Au_{38}O_2$−CO−B and $Au_{38}O_2$−CO−C) also implies a lower reactivity toward CO oxidation. In fact, it was not possible to find any transition state leading to CO_2 formation. This means that, in gold nanoparticles with a low oxygen coverage, CO will preferentially adsorb on the nonreactive B and C positions, and only when the nanoparticle becomes covered by an oxide layer will the reactivity toward CO oxidation increase.

3.4. Macroscopic Approach. Oxygen activation is an important step for catalytic oxidation reactions, and it has been experimentally and theoretically studied in detail in the above sections. Going one step further, we have studied their reactivity toward specific molecules, and in particular, we have considered the epoxidation of styrene due to its industrial and academic interest. Furthermore, oxirane groups are highly reactive, which makes epoxides important organic intermediate compounds in the synthesis of fine chemicals. Au NPs supported on a range of oxides have already been used for the epoxidation of styrene using tertiary butyl hydroperoxide (TBHP) as oxidant.[67−69] However, the use of molecular O_2 as an environmental friendly oxidant is highly interesting and will be considered in our case.

The catalytic behavior of different Au−MWCNT samples in the epoxidation of styrene with molecular oxygen as oxidant is shown in Table 4. The best catalytic performance has been observed for the 0.3Au−CNT sample with 0.9 nm particle diameter, while no catalytic activity has been observed on the Au−CNT sample with a particle size of 4 nm. The absence of catalytic behavior in the last case is due to the inability of gold within larger crystallites to activate molecular oxygen. On the other hand, TEM studies of the catalysts after reaction show a great tendency of gold to agglomerate under reaction conditions (Figure 10). This was avoided, or at least minimized, by using low gold content and optimizing the citrate/Au molar ratio. While it has been indicated above that citrate ions are necessary in the synthesis of Au−MWCNT, if their amount is too high, then citrate ions could block the gold surface, decreasing its reactivity (Figure 11). Citrate ions have been shown to be stable under reaction conditions (see Figure S3 in the Supporting Information). On the other hand, a low amount of citrate ions favors a fast aggregation of the Au NPs during

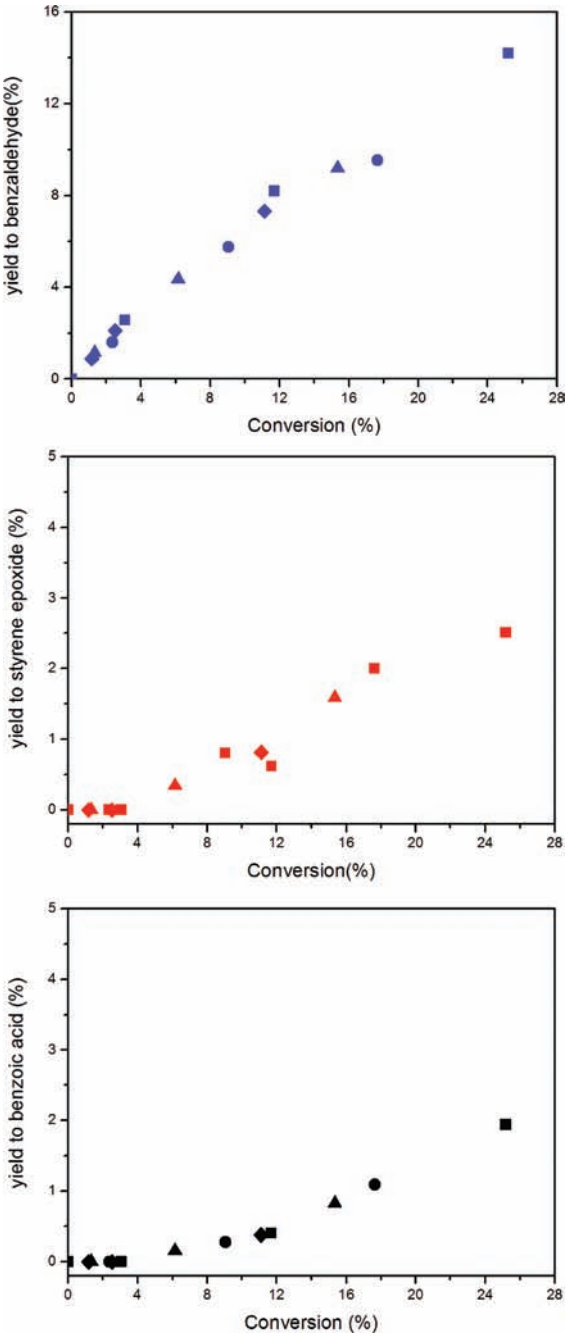

Figure 12. Yield to benzaldehyde, styrene epoxide, and benzoic acid versus styrene conversion obtained on 0.3Au−CNT (■), 3Au−CNT (●), 3Au−CNT[a](◆), and 15Au−CNT (▲) catalysts. [a]Citrate/Au molar ratio = 600.

catalytic performance, decreasing their activity accordingly (see entry 3 in Table 4). Indeed, the low catalytic activity observed with the samples at Au wt % > 0.3 can be associated to a sintering of the gold NPs under reaction conditions, as observed from the histograms derived by TEM analysis shown in Figure 10. In the absence of sintering of gold NPs (sample 0.3Au−CNT), a high intrinsic catalytic activity can be observed. The rate of 0.038 mol styrene/h g on the 0.3Au−CNT sample with 0.9 nm gold particle size is twice more active than the values obtained for the so-called "magic" Au_{55} gold particles.[43]

With respect to the selectivity of the process, benzaldehyde, styrene epoxide, benzoic acid, acetophenone, and CO_2 are observed together with minor amounts of heavier reaction products, probably formed by styrene polymerization. By following the yields of the different products versus styrene conversion (Figure 12), similar product distributions are observed with all samples. According to the product distribution profile, benzaldehyde is a primary product, while styrene epoxide, benzoic acid, and acetophenone are secondary products. Benzoic acid appears simultaneously with styrene epoxide formation, while acetophenone is formed only at high styrene conversions.

The reaction mechanism for styrene oxidation on oxygen preadsorbed Au(111) surface has been studied by DFT calculations,[70] and two possible oxametalacycle intermediates have been postulated by producing styrene epoxide and phenyl acetaldehyde as the most stable products and benzaldehyde and a $-CH_2-$ fragment as less stable species. Similar mechanistic insights into the selective epoxidation of styrene on Au(111) have been also drawn by Friend et al.,[71] who, contrary to our results, did not detect benzaldehyde in their experiments. On the other hand, oxidative cleavage of styrene into benzaldehyde and formaldehyde has been associated in the literature with the formation of peroxo species on TiO_2 and TiO_2/SiO_2 catalysts[72] or to the formation of metal−oxo radicals on transition-metal complexes.[73] Once formed, the aldehyde acts as a coreactant in the epoxidation of the alkene (styrene), in the presence of molecular O_2, according to a peracid mechanism and/or acylperoxo radical mechanism. In our case, the formation of benzaldehyde as primary product and epoxide together with benzoic acid as secondary products points to the latter possible reaction mechanism, in which benzaldehyde, once formed, acts as a coreactant in the epoxidation of styrene. However, the nature of the active oxygen species responsible for the initial formation of benzaldehyde from styrene (atomic oxygen involved in the formation of an oxametalacycle intermediate or a peroxo species) remains unsolved at the moment, and further work trying to clarify this point is in progress.

4. CONCLUSIONS

1 A technique has been developed to prepare small (0.9−1.5 nm) gold nanoclusters in a very narrow size distribution (1.1 ± 0.5 nm) onto multiwalled carbon nanotubes at room temperature.
2 DFT calculations indicate that small Au_{38} nanoparticles can dissociate at least 12 O_2 molecules with low activation barriers producing stable $Au_{38}O_{16}$ and $Au_{38}O_{24}$ oxidized particles, this finding being experimentally supported by XPS spectroscopy.
3 $^{16}O_2/^{18}O_2$ isotopic exchange experiments confirm that small (0.9−1.5 nm) gold nanoparticles are able to dissociate O_2 at room temperature and to be oxidized, while O_2 dissociation does not occur on larger gold particles (4 nm) and they are not oxidized.
4 $^{16}O_2/^{18}O_2$ isotopic exchange experiments and DFT calculations show that O_2 dissociation is faster than recombination and desorption of O_2, which explains the possibility to stabilize small gold oxide particles.
5 It is found from CO titration and DFT calculations that the small (0.9−1.5 nm) oxidized nanoparticles can reversibly transfer and uptake oxygen, behaving as an oxide catalyst for oxidation reactions.
6 The oxidized gold nanoparticles are active for styrene oxidation with air, giving benzaldehyde and styrene epoxide.

■ ASSOCIATED CONTENT

Supporting Information. Additional information as noted in the text. This material is available free of charge via the Internet at http://pubs.acs.org.

■ AUTHOR INFORMATION

Corresponding Author
acorma@itq.upv.es; ernest.mendoza@upc.edu

■ ACKNOWLEDGMENT

Financial support by the Spanish MICINN (MAT2009-14528-C02-01 and PLE2009-0046) and CONSOLIDER Ingenio 2010-MULTICAT is gratefully acknowledged. We thank Generalitat Valenciana for funding through the PROMETEO project 2088/130 amd Generalitat de Catalunya for funding though the project VALTEC 09-01-0043. L.A. thanks the Centre de Recerca en Nanoenginyeria of the Universitat Politécnica de Catalunya for the predoctoral fellowship and B.B. thanks MICINN for the PTA2008-1108-I contract. We thank Red Española de Supercomputación (RES) and Centre de Càlcul de la Universitat de València for computational resources and technical assistance.

■ REFERENCES

(1) Grassian, V. H. *J. Phys. Chem. C* **2008**, *112*, 18303.
(2) Lei, Y.; Mehmood, F.; Lee, S.; Greeley, J.; Lee, B.; Seifert, S.; Winans, R. E.; Elam, J. W.; Meyer, R. J.; Redfern, P. C.; Teschner, D.; Schlogl, R.; Pellin, M. J.; Curtiss, L. A.; Vajda, S. *Science* **2010**, *328*, 224.
(3) Park, J. B.; Graciani, J.; Evans, J.; Stacchiola, D.; Senanayake, S. D.; Barrio, L.; Liu, P.; Sanz, J. F.; Hrbek, J.; Rodriguez, J. A. *J. Am. Chem. Soc.* **2010**, *132*, 356.
(4) Wang, J. X.; Inada, H.; Wu, L. J.; Zhu, Y. M.; Choi, Y. M.; Liu, P.; Zhou, W. P.; Adzic, R. R. *J. Am. Chem. Soc.* **2009**, *131*, 17298.
(5) Binder, A.; Seipenbusch, M.; Muhler, M.; Kasper, G. *J. Catal.* **2009**, *268*, 150.
(6) Desikusumastuti, A.; Happel, M.; Qin, Z.; Staudt, T.; Lykhach, Y.; Laurin, M.; Shaikhutdinov, S.; Rohr, F.; Libuda, J. *J. Phys. Chem. C* **2009**, *113*, 9755.
(7) Dudin, P.; Barinov, A.; Gregoratti, L.; Scaini, D.; He, Y. B.; Over, H.; Kiskinova, M. *J. Phys. Chem. C* **2008**, *112*, 9040.
(8) Haruta, M.; Kobayashi, T.; Sano, H.; Yamada, N. *Chem. Lett.* **1987**, 405.
(9) Haruta, M. *Catal. Today* **1997**, *36*, 153.
(10) Hughes, M. D.; Xu, Y. J.; Jenkis, P.; McMorn, P.; Landon, P.; Enache, D. I.; Carley, A. F.; Attard, G. A.; Hutchings, G. J.; King, F.; Stitt, E. H.; Johnston, P.; Griffin, K.; Kiely, C. J. *Nature* **2005**, *437*, 1131.
(11) Enache, D. I.; Edwards, J. K.; Landon, P.; Solsona-Espriu, B.; Carley, A. F.; Herzing, A. A.; Watanabe, M.; Kiely, C. J.; Knight, D. W.; Hutching, G. J. *Science* **2006**, *311*, 362.

(12) Valden, M.; Lai, X.; Goodman, D. W. *Science* **1997**, *281*, 1647.
(13) Abad, A.; Corma, A.; García, H. *Chem.—Eur. J.* **2008**, *14*, 212.
(14) Nijhuis, T. A.; Visser, T.; Weckhuysen, B. M. *Angew. Chem., Int. Ed.* **2005**, *44*, 1115.
(15) Claus, P. *Appl. Catal. A: Gen.* **2005**, *291*, 222.
(16) Hugon, A.; Delannoy, L.; Louis, C. *Gold Bull.* **2008**, *41*, 127.
(17) Yang, X. F.; Wang, A. Q.; Wang, Y. L.; Zhang, T.; Li, J. *J. Phys. Chem. C* **2010**, *114*, 3131.
(18) Corma, A.; Serna, P. *Science* **2006**, *313*, 332.
(19) Boronat, M.; Concepción, P.; Corma, A.; González, S.; Illas, F.; Serna, P. *J. Am. Chem. Soc.* **2007**, *129*, 16230.
(20) Corma, A.; Concepción, P.; Serna, P. *Angew. Chem., Int. Ed.* **2007**, *46*, 7266.
(21) Juarez, R.; Concepción, P.; Corma, A.; Fornés, V.; Garcia, H. *Angew. Chem., Int. Ed.* **2010**, *49*, 1286.
(22) QFu, Q.; Saltsburg, H.; Flytzani-Stephanopoulos, M. *Science* **2003**, *301*, 935.
(23) Rodriguez, J. A.; Ma, S.; Liu, P.; Hrbek, J.; Evans, J.; Perez, M. *Science* **2007**, *318*, 1757.
(24) Hashmi, A. S. K.; Weyrauch, J. P.; Rudolph, M.; Kurpejovic, E. *Angew. Chem., Int. Ed.* **2004**, *43*, 6545.
(25) Carrettin, S.; Guzmán, J.; Corma, A. *Angew. Chem., Int. Ed.* **2005**, *44*, 2242.
(26) González-Arellano, C.; Corma, A.; Iglesias, M.; Sánchez, F. *Chem. Commun.* **2005**, 3451.
(27) González-Arellano, C.; Abad, A.; Corma, A.; García, H.; Iglesias, M.; Sánchez, F. *Angew. Chem., Int. Ed.* **2007**, *46*, 1536.
(28) Gottfried, J. M.; Schroeder, S. L. M.; Schmidt, K. J.; Christmann, K. *Surf. Sci.* **2002**, *511*, 65.
(29) Canning, N. D. S.; Outka, D.; Madix, R. J. *Surf. Sci.* **1984**, *141*, 240.
(30) Deng, X.; Min, B. K.; Guloy, A.; Friend, C. M. *J. Am. Chem. Soc.* **2005**, *127*, 9267.
(31) Stiehl, J. D.; Kim, S. T.; McClure, S. M.; Mullins, C. B. *J. Am. Chem. Soc.* **2004**, *126*, 1606.
(32) Deng, X.; Friend, C. M. *J. Am. Chem. Soc.* **2005**, *127*, 17178.
(33) XDeng, X.; Min, B. K.; Liu, X. Y.; Friend, C. M. *J. Phys. Chem. B.* **2006**, *110*, 15982.
(34) Min, B. K.; Alemozafar, A. R.; Pinnaduwage, D.; Deng, X.; Friend, C. M. *J. Phys. Chem. B.* **2006**, *110*, 19833.
(35) Roldán, A.; Gonzalez, S.; Ricart, J. M.; Illas, F. *Chem. Phys. Chem* **2009**, *10*, 348.
(36) López, N.; Janssens, T. V. J.; Clausen, B. S.; Xu, Y.; Mavrikakis, M.; Bligaard, T.; Nørskov, J. K. *J. Catal.* **2004**, *223*, 232.
(37) Boronat, M.; Corma, A. *Dalton Trans.* **2010**, *39*, 8538.
(38) Mills, G.; Gordon, M. S.; Metiu, H. *J. Chem. Phys.* **2003**, *118*, 4198.
(39) Yoon, B.; Häkkinen, H.; Landman, U. *J. Phys. Chem. A* **2003**, *107*, 4066.
(40) Jiang, T.; Mowbray, D. J.; Dobrin, S.; Falsig, H.; Hvolbæk, B.; Bligaard, T.; Nørskov, J. K. *J. Phys. Chem. C* **2009**, *113*, 10548.
(41) Herzing, A. A.; Kiely, C. J.; Carley, A. F.; Landon, P.; Hutchings, G. J. *Science* **2008**, *321*, 1331.
(42) Chen, M. S.; Goodman, D. W. *Science* **1998**, *281*, 1647.
(43) Turner, M.; Golovko, V. B.; Vaughan, O. P.H.; Abdulkin, P.; Berenguer-Murcia, A.; Tikhov, M. S.; Johnson, B. F. G.; Lambert, R. M. *Nature* **2008**, *454* (7207), 981.
(44) Zope, B. N.; Hibbitts, D. D.; Neurock, M.; Davis, R. J. *Science* **2010**, *330*, 74.
(45) Van Bokhoven, J. A.; Louis, C.; Miller, J. T.; Tromp, M.; Safonova, O. V.; Glatzel, P. *Angew. Chem., Int. Ed.* **2006**, *45*, 4651.
(46) Miller, J. T.; Kropf, A. J.; Zha, Y.; Regalbuto, J. R.; Delannoy, L.; Louis, C.; Bus, E.; van Bokhoven, J. A. *J. Catal.* **2006**, *240*, 222.
(47) Weither, N.; Beesley, A. M.; Tsapatsaris, N.; Delannoy, L.; Louis, C.; van Bokhoven, J. A.; Schroeder, S. L. M. *J. Am. Chem. Soc.* **2007**, *129*, 2240.
(48) Vannice, M. A. *Catal. Today* **2007**, *123*, 18.
(49) Comotti, M.; Li, W. C.; Spliethoff, B.; Schuth, F. *J. Am. Chem. Soc.* **2006**, *128*, 917.
(50) Shimizu, K.; Miyamoto, Y.; Kawasaki, T.; Tanji, T.; Tai, Y.; Satsuma, A. *J. Phys. Chem. C* **2009**, *113*, 17803.
(51) Gross, E.; Asscher, M.; Lundwall, M.; Goodman, D. W. *J. Phys. Chem.C* **2007**, *111*, 16197.
(52) Perdew, J. P.; Chevary, J. A.; Vosko, S. H.; Jackson, K. A.; Pederson, M. R.; Singh, D. J.; Fiolhais, C. *Phys. Rev. B* **1992**, *46*, 6671.
(53) Perdew, J. P.; Wang, Y. *Phys. Rev. B* **1992**, *45*, 13244.
(54) Kresse, G.; Furthmüller, J. *Phys. Rev. B* **1996**, *54*, 11169.
(55) Kresse, G.; Hafner, J. *Phys. Rev. B* **1993**, *47*, 558.
(56) Blöchl, P. E. *Phys. Rev. B* **1994**, *50*, 17953.
(57) Heyden, A.; Bell, A. T.; Keil, F. J. *J. Chem. Phys.* **2005**, *123*, 224101.
(58) Henkelman, G.; Jónsson, H. *J. Chem. Phys.* **1999**, *111*, 7010.
(59) Sanville, E.; Kenny, S. D.; Smith, R.; Henkelman, G. *J. Comput. Chem.* **2007**, *28*, 899.
(60) Henkelman, G.; Arnaldsson, A.; Jónsson, H. *Comput. Mater. Sci.* **2006**, *36*, 254.
(61) Newman, J. D. S.; Blanchard, G. J. *Langmuir* **2006**, *22*, 5882.
(62) Correa-Duarte, M. A.; Sobal, N.; Liz-Marzán, L. M.; Giersig, M. *Adv. Mater.* **2004**, *16*, 2179.
(63) Knecht, J.; Fischer, R.; Overhof, H.; Hensel, F. *J. Chem. Soc. Chem. Commun.* **1978**, *21*, 905.
(64) Zwijnenburg, A.; Goossens, A.; Sloof, W. G.; Crajé, M. W. J.; van der Kraan, A. M.; John, L. J.; Makkee, M.; Moulijn, J. A. *J. Phys. Chem. B.* **2002**, *106*, 9853.
(65) Chusuei, C. C.; Lai, X.; Luo, K.; Goodman, D. W. *Top. Catal.* **2001**, *14*, 71.
(66) Zafeiratos, S.; Kennou, S. *Surf. Sci.* **1999**, *443*, 238.
(67) Liu, J.; Wang, F.; Xu, T.; Gu, Z. *Catal. Lett.* **2010**, *134*, 51.
(68) Yin, D.; Qin, L.; Liu, J.; Jin, C. L. Y. *J. Mol. Catal. A. Chem* **2005**, *240*, 40.
(69) Choudhary, V. R.; Durnbre, D. K. *Catal. Commun* **2009**, *10*, 1738.
(70) Xue, L. Q.; Pang, X. Y.; Wang, G. C. *J. Comput. Chem.* **2009**, *30*, 438.
(71) Quiller, R. G.; Liu, X.; Friend, C. M. *Chem. Asian J.* **2010**, *5*, 78.
(72) Nie, L.; Xin, K. K.; Li, W. S.; Zhou, X. P. *Catal. Commun.* **2007**, *8*, 488.
(73) Wentzel, B. B.; Gosling, P. A.; Feiters, M. C.; Nolte, R. J. M. *J. Chem. Soc., Dalton Trans.* **1998**, 2241.